This is a preprint, the final version is subject to change, of the American Mineralogist (MSA)
Cite as Authors (Year) Title. American Mineralogist, in press.
(DOI will not work until issue is live.) DOI: http://dx.doi.org/10.2138/am.2013.4204

DFT+U investigation of the catalytic properties of ferruginous clay

Dawn L. Geatches,[1*] Stewart J. Clark,[1] and Hugh C. Greenwell[2]

[1] Durham University, Physics Dept., South Road, Durham. DH1 3LE. UK.

[2] Durham University, Earth Sciences Dept., South Road, Durham. DH1 3LE. UK.

Abstract

The formation of fossil oil within clay minerals i.e. mineral-catalyzed decarboxylation, is a mechanism awaiting a thorough chemical explanation. To contribute to such an explanation, the study presented here investigates this mechanism at the level of first principles, electronic structure computations, employing density functional theory (DFT plus Hubbard - U), planewaves, pseudopotentials and periodic cells of two types of ferruginous clay minerals, specifically two types of nontronite ($Fe_2(Si,Al)_4O_{10}(OH)_2$). The formation of the fossil oil is modelled as a decarboxylation pathway, converting the fatty acid propionic acid, C_2H_5COOH to an alkane, C_2H_6 and the intermediate stages along this conversion pathway are represented by five configurations of interlayer species within the clay minerals. In this study we test both the

*Corresponding author, Tel: +44 (0)191 3343549; email: d.l.geatches@dur.ac.uk

effect of the presence of iron on the theoretical stages of decarboxylation, together with the effect of two different density functionals: with and without strong correlations of the d-orbital electrons of iron. We have found that inclusion of the d-orbital electron correlations in the guise of a Hubbard parameter results in the introduction of three new intermediate configurations, (one of which is potentially a new transition state) alters the location of the occupied Fermi level orbitals, and changes the band gaps of the clay mineral/interlayer species composites, all of which serves to inform the chemical interpretation of mineral-catalyzed decarboxylation.

Keywords: DFT, Hubbard value, oil formation, iron-bearing clay minerals

INTRODUCTION

Almon and Johns (1975) performed a series of experiments designed to elucidate the chemical pathway describing the formation of fossil oil within clay minerals. The abundance of iron-bearing clay minerals comprising the bulk of our Earth (Greenwood and Earnshaw 1994; Morgan and Anders 1980) makes it highly probable that these clays were hosts to fossil oil formation and hence decarboxylation. Almon and Johns were of the same opinion as a type of iron-bearing clay mineral, nontronite, ($Fe_2(Si,Al)_4O_{10}(OH)_2$) was one of their experimental minerals. From the results of their experiments, Almon and Johns hypothesised a reaction comprising five stages of the decarboxylation pathway within the interlayer space of a clay mineral, from the initial reactant stage of a fatty acid (propionic acid, C_2H_5COOH) to the end product stage of an alkane (C_2H_6) with three intermediate stages in-between. The

motivation for examining the catalytic effect of various clay minerals in this decarboxylation mechanism, derives from the similarity between the fatty acids of the fossilised biological matter and those within the crops used as biofuel feedstocks, hence this study has the potential to inform and eventually improve the efficiency of the production of biofuels.

A clay mineral layer is formed by the conjoining of a tetrahedral silicate sheet — general form Si_4O_6 — to an octahedrally coordinated metal oxide sheet, which in nontronite is $Fe_4O_8(OH)_4$. The ratio of tetrahedral to octahedral sheets describes this coordination e.g. nontronite is a 2:1 dioctahedral phyllosilicate, i.e. there is one octahedral metal oxide sheet sandwiched between two tetrahedrally coordinated silicate sheets where the octahedral sheet contains the species Fe^{3+}. The tetrahedral or basal surfaces often contain substitutions where the charge deficit introduced by substitution of Fe^{3+} or Al^{3+} for Si^{4+} is balanced by an interlayer cation. Nontronites with a basal surface substitution of $\frac{1}{8}$ Fe^{3+} or Al^{3+} are type NG-1 and ideal, respectively. The space between the layers of clay minerals is host to a variety of ions such as cations sodium, calcium and potassium as well as organic molecules such as fatty acids and hydrocarbons. The variety of the chemical environment of all clay mineral surfaces, including edges as well as basal surfaces, together with that of the interlayer species, are thought to be responsible for catalyzing chemical reactions such as the decarboxylation of a fatty acid into an alkane. In this study we examine the basal surfaces only, and therefore will not be capturing the full potential reactivity of the ferruginous clays, a comprehensive study of which is beyond the scope of this investigation.

Along a chemical reaction pathway there generally exists intermediate configurations* of chemically reactive species, some of which might be transition states. Their identification is important due to the information they yield regarding chemical reaction activation energies and the relative stability of products. Transition states exist at saddle points in the energy landscape of systems, and can be captured computationally by accurate optimization of atomic coordinates. By assuming that the three hypothesised intermediate configurations of Almon and Johns (1975) are potential transition states, we posit that accurate optimization of these initial configurations allows them to either become further refined, resulting in optimised configurations that resemble their pre-optimised structures, (or configurations other than the reactant or product) or, if the initial models are not potential transition states, their optimised configurations will have changed to the reactant or product models only. That is, if an optimised groundstate configuration is different to those of the reactant and/or product, it will be assumed to be a new intermediate configuration and hence a potential transition state, which, if supported by further analysis could be verified definitively by vibrational analysis determining a sole imaginary eigenfrequency (Geatches et al. 2010).

Examining the catalytic role of iron-containing clay minerals is complicated by iron being a transition metal, (electronic structure $[Ar]4s^2 3d^6$) where the unpaired electrons in five of the d-orbitals could be strongly correlated. Consequently, there is a complex interplay of Coulomb and exchange interactions between the 3-d electrons,

*In this study we have not made a distinction between 'intermediate', 'intermediate stage' or 'intermediate configuration'. Throughout the discussion where any of these three terms are used, they refer to configurations that are potential transition states, as opposed to 'intermediates' in the chemical sense, which are distinctly different to transition states.

which the generalised gradient approximation (GGA) functional is not fully able to capture as it may not split the triply degenerate d_{zx}, d_{yz} and d_{xy}, i.e. the t_{2g} bands (Fang et al. 1999). The implications for this are that an iron oxide bearing insulator for example, could be described as metallic within the GGA approximation. The strong correlations of the d-electrons can be modelled with the addition of a Hubbard-type model, which is used in addition to the GGA (and the local density approximation — LDA — functional). A description of the addition of the Hubbard parameter to the LDA functional details the principle of its application (Anisimov et al. 1997).

Iron comprises a major constituent of many different materials from the biological to the geophysical, and the effect of the Hubbard parameter on the d-electrons of iron within DFT has been examined in many of these systems, such as the molecular environment in iron porphyrins (Panchmatia et al. 2007), the redox potentials for batteries (Zhou et al. 2004), model industrial catalysts such as $FeSbO_4$, used for selective oxidation (Grau-Crespo et al. 2006), materials comprising containers for the storage of spent radioactive substances (Rák et al. 2011), minerals such as mackinawite, (FeS) (Devey et al. 2008) and fayalite, (Fe_2SiO_4) found in the Earth's upper mantle (Cococcioni et al. 2003) and oxygen storage in iron-modified cerium oxide (Chen and Chang 2011). In each of these cases, apart from in the examination of the bulk and surface structures and properties of mackinawite, it was found that the addition of a Hubbard parameter produced more physically realistic results compared to the computations without this parameter. Although there are many examples of the application of DFT+U for iron-bearing minerals demonstrating the necessity of

the inclusion of the Hubbard parameter, (Devey et al. 2009; Hsu et al. 2010; Kiejna and Pabisiak 2012; Stashans et al. 2012) and its importance in the investigation of transition metal oxide surface/interface interactions is well-established, (Nolan et al. 2006, 2008, 2012; Branda et al. 2010; Szabová et al. 2010) the application to date, of the Hubbard parameter to clay minerals appears to be in its infancy, with our study apparently among the first in this particular field.

Although there is general agreement regarding the benefits of employing the Hubbard parameter for materials containing the strongly correlated d-electrons of iron and also for the f-electrons of materials such as ceria (Hernández et al. 2009), there is no consensus on the most appropriate U value for iron, which varies from 3.71eV for Fe^{2+} to 4.9eV for Fe^{3+} in olivine (Zhou et al. 2004). The examples previously cited illustrate that the most appropriate U value for iron strongly depends on the environment. One study tested $U = 4.3$eV and $U = 6.1$eV and determined that $U = 4.3$eV was more appropriate for iron in a garnet structure (Rák et al. 2011), which contains similar iron-silicon-oxygen environments to those within nontronite. There is broad agreement between the DFT+U studies that whether iron is in octahedral or tetrahedral coordination, a U value of between 4.0eV and 4.9eV will yield optimal results, i.e. those that are verifiable experimentally. One study suggests that higher valence states lead to higher U values and that this aspect of the electronic structure of iron-containing materials becomes especially important when investigating mechanisms involving the transfer of electrons between states of different kinds, e.g. the catalysis of organic molecules on transition metal surfaces (Zhou et al. 2004), which is comparable to the study we present here.

The method of implementing the Hubbard parameter varies from an ab initio technique that is able to evaluate U for an atom in different environments (Mosey and Carter 2007), to self-consistent perturbation methods (Zhou et al. 2004), to using empirical values and checking the resulting density of states (Grau-Crespo et al. 2007). There also exists a method that does not explicitly calculate a Hubbard parameter, but carries out standard DFT calculations under the GGA exchange-correlation functional, followed by the partial removal of electrons, further details of which can be found in the work of Cococcioni et al. (2003). Our method of choice for the Hubbard parameter was based on the results gained from investigating it in a simpler system and attempting to reproduce the optical band gap of FeO, which is 2.4eV (Gramsch et al. 2003). An optical band gap measures the difference between the ionisation energy and electron affinity, which for Fe involves the promotion of a 3d electron to the 4s orbital, whereas DFT uses Kohn-Sham eigenvalues to increase the separation of the d-orbitals via application of a Hubbard value, thereby creating a band gap between the d-orbitals. Although the experimental and theoretical origins of the band gap differ (Ashcroft and Mermin 1976), the experimental values in the case of composite iron within clay minerals are our only physical guides, at present. How we determined the most appropriate U value for our investigation will be explained in the following section. Our resulting U value falls within the documented range for Fe from $U = 4$ to 7eV (Fang et al. 1999; Pickett et al. 1998) and thus within the ranges of the references previously cited.

To determine whether the inclusion of a description of the strongly correlated d-electrons of iron would produce a potential new transition state, we created two sets

of models, each set describing a type of nontronite and each reproducing the reactant, product and three intermediate stages in the decarboxylation pathway hypothesised by Almon and Johns (1975). We then allowed these models to relax under two density functionals, GGA and GGA+U. By analysing the resulting configurations, total energy differences, Fermi level orbital occupancies and band gaps, we determined whether a potential new transition state had been located.

MODELS AND COMPUTATIONAL DETAILS

Models

Our previous study into pyrophillite-like smectites and their interlayer guests showed that the optimal environment for decarboxylation to occur comprised an aluminum substitution in the tetrahedral sheet/basal surface, which is thought to be the site of catalytic activity (Almon and Johns 1975), plus a sodium atom in the interlayer, which counterbalances the charge generated by the substitution and enables electron transfer between the guest organic molecule and the clay host.

The optimal model from our previous study into decarboxylation within a pyrohillite-like clay mineral (Geatches et al. 2010), $(Al_2Si_4O_{10}(OH)_2)_2$, space group $P\bar{1}$, was used as the template model for this study. All octahedral Al were substituted by Fe and in one labelled Ideal, the Al substitution in the tetrahedral sheet remained, in the second, labelled NG-1, the tetrahedral Al was also substituted by Fe. Both models contained Na in the interlayer as the charge-balancing cation as shown in Figure 1. The size of the unit cell used in this investigation allowed for a $\frac{1}{4}$ substitution of

Fe^{3+} for Si^{4+} in a basal surface, which is double the proportion found in the physical clay. As a substitution ratio of $\frac{1}{8}$ would require double the cell size, and hence up to eight times the computational load, we only use a smaller cell with a higher proportion of basal site substitutions. This ensured that the potential catalytic effect of the substitution was optimised without loss of generality, that is, if the site of the substitution in the tetrahedral sheet, together with the cation, is important for a reaction to occur, then the environment modelled by a single unit cell will exist within a double cell without loss of any detail.

Computational details

We employed the CASTEP (Clark et al. 2005) code, with a planewave basis set within the DFT formalism (Kohn and Sham 1965). Convergence testing showed that a planewave basis represented by a kinetic energy cut-off of 550eV gave an energy difference in total energies of less than 0.04eV per unit cell for higher cut-offs. The Brillouin zone integrations were performed on a grid containing two k-points giving an energy difference of 0.03eV per unit cell between two and four or five k-points and, as this is within the energy cut-off criteria, two k-points were adequate to converge the calculation at a volume appropriate for these simulations.

We used the generalized gradient approximation (GGA) density functional, specifically Perdew, Burke and Ernzerhof (PBE) (Perdew et al. 1996) as this describes molecular bonding to a greater accuracy than does the local density approximation (LDA). PBE ultrasoft pseudopotentials (Vanderbilt, D. 1990) were used as these are consistent with the PBE exchange functional, and for iron this included the

PBE exchange-correlation functional with core corrections (Louie et al. 1982). The (geometry) optimizer was Broyden-Fletcher-Goldfarb-Shanno (BFGS) and the electronic method was ensemble density functional theory (EDFT) (Mazari et al. 1997). Further convergence details per BFGS iteration are as follows:- energy change per ion: dE/ion 10^{-5}eV; maximum force: $|F|$max 0.03 eV/$\mathring{A}$; change in distance: $|dR|$ 0.001$\mathring{A}$. All calculations were spin-polarised.

We determined a suitable U value for the nontronite models by investigating the effect on the band gap of wüstite — a crystalline form of FeO — with the U value ranging from 2.0eV to 6.0eV. Wüstite contains iron in its more electron dense form in comparison to ferric iron. There are potentially both types in the clay models, iron (III) in the octahedral sheet of Ideal and NG-1, and iron (II) in the tetrahedral sheet of NG-1. By investigating the Hubbard parameter for the most d-electron dense form of iron, and hence potentially the most strongly correlated d-electrons, we are assuming that we are accounting for the less d-electron dense iron at the same time.

We used the same computational parameters as previously detailed apart from increasing the number of k-points due to the smaller cell size of wüstite, and reasoned that the results from this computationally inexpensive iron oxide crystal would be somewhat transferable to the larger clay models due to the presence of FeO in the clay layers. As mentioned in the Introduction, although the origins of an experimental and theoretical band gap differ, the former provides the only physical guidance to reducing the strong correlation between the d-orbital electrons of iron. We found that the Hubbard parameter corresponding to a band gap of 2.4eV was $U = 5.0$eV, which closely agrees with the result of $U = 4.9$eV for FeO obtained by self-consistent

perturbation methods (Zhou et al. 2004). Consequently, $U = 5.0$eV was applied to all iron atoms in both Ideal and NG-1 nontronite.

The Ideal and NG-1 models were allowed to completely relax both with and without the inclusion of the Hubbard parameter. Initial relaxation involved both the cell and contents after which the $c-$length was extended to $14.5\mathring{A}$ to allow for the inclusion of a gallery guest, see Figure 1.

The optimised Ideal and NG-1 models were used to produce the five configurations as shown in Figure 2, following the principle that, if any of the postulated intermediates were transition states then, allowing them to relax would result in the reproduction of either the initial configuration or another one that differed from the Reactant and Product models. All of the cell contents were allowed to relax with the lattice parameters held fixed, with the same convergence criteria as detailed previously. A post-processing band structure calculation to enable visualisation of Fermi level orbital occupancies, completed the computations.

RESULTS AND DISCUSSION

PBE-GGA

The relaxed configurations for the intermediate stages of both Ideal and NG-1 (Figure 3) under the GGA-only functional, have all assumed the Reactant configuration, hence, within these ferruginous clay mineral models, no potential transition state has been found.

The Product models for Ideal and NG-1 are both lower in energy than their respec-

tive Reactant models and the energy differences are an order of magnitude larger than the tolerance criteria, hence the conversion from Reactant to Product is possible, which suggests that a chemical reaction (such as decarboxylation) is feasible within these environments. The energy differences shown in Table 1 provide information about the energies of relative orientations of the fatty acid to the clay layer. In both Ideal and NG-1, Stage 1, where the carboxyl head has relaxed to point away from the layer, the difference in energy between this orientation and that of the Reactant is positive, hence the Reactant model is closer to the global minimum for this system. This is useful information because it emphasises the dependence of the outcome of a geometry optimization on the configuration of the initial input. If this 'falling into local minima' were of concern, then by testing a few orientations, an energy/orientation picture could emerge.

Stage 2 in both Ideal and NG-1 is closer to the global minimum than the original Reactant models because their energy differences ($E_{s2}-E_r$) are negative. Although this does not affect the conclusion drawn from the results of these geometry optimizations, insofar as none of the initial configurations are transition states as they relaxed away from their starting configurations, this orientation information could be used in, for example, the search for a transition state where the Reactant model[†] would be that of the optimised NG-1, Stage 2 as this has the lowest energy of the reactant configurations shown here.

Scrutiny of the Fermi level orbitals (Figure 3) shows the occupied orbitals are those of the iron within the octahedral sheet, apart from Stage 3 of Ideal and Stage 1 of

[†]The two end configurations of a reaction pathway in a transition state search implemented in CASTEP, are called the 'Reactant' and 'Product'.

NG-1 where there is involvement of the oxygen in the octahedral sheet lying above the Al substitution in the tetrahedral sheet. There is no involvement of the fatty acid and alkane, which indicates that, on application of energy, their electrons would not be the first to respond, hence although earlier analysis of the energy differences indicated the possibility of a chemical reaction within these environments, a decarboxylation reaction is not a high probability within these clays. If it were, then the Fermi level orbitals would be occupied on the interlayer species. This localisation of the Fermi orbitals within the clay layer could be due to the absence of the Hubbard parameter, therefore, can the results be described as 'real' results or are they artefacts of the exchange-correlation functional used?

Examining the band gaps of the optimised models (Table 2) illustrates that without inclusion of a Hubbard parameter, the ferruginous clay minerals are described as being more metallic in nature than insulating. In seven out of the ten nontronite models, the band gap is an order of magnitude less than in the similar aluminosilicates. The inability of the GGA-only functional to describe the strong correlations of the d-electrons of iron, has resulted in a reduction of the band gap in all cases in comparison with the aluminium-bearing clay models.

PBE-GGA+U

There is no data available for Stage 1 of both Ideal and NG-1 because the energy minimisation procedure resulted in a deviation away from the original minimum into another minima, not based on the starting configuration. This implied that the

starting configuration was so far removed from an energy minimum, that the results would have little bearing on the relevance of Stage 1's initial configuration and how close this was to a possible transition state. It could be said that the problem with Stage 1 indicates the unlikelihood of it being a transition state, however, exactly the same configurations had no problem converging in the absence of the Hubbard value. Forces between some of the atoms suggest that in this configuration the Hubbard parameter created large Coulomb forces between some electrons. Within this study we are comparing models relaxed under GGA and GGA+U, therefore this result suffices to say that with the application of the Hubbard parameter, the potential for Stage 1 to be a transition state in the decarboxylation pathway within Ideal and NG-1 is ruled out.

As in the case of the GGA-only calculations, the negative energy differences between the Reactant and Product shown in Table 3 imply that these clay mineral environments are potential hosts to chemical reactions and hence possibly decarboxylation. Ideal, Stage 3 and NG-1, Stage 2 would not converge to the same precision as the others in all of the three convergence criteria. Ideal, Stage 3 converged to an order of magnitude less in all three criteria, and NG-1, Stage 2 met the convergence criteria for dE/ion and $|F|$max but not $|dR|$. Their progress was monitored at various intervals and their inclusion in the results is representative of their converged results, and where it is thought that convergence to the imposed criteria would make a difference, reference is made to this in the text.

As Stage 2 in Ideal and NG-1 and Stage 3 of NG-1 have lower energies than the Reactant, they could not be transition states of our proposed decarboxylation pathway.

The higher energy of Ideal, Stage 3 is possibly due to its relatively lower convergence as discussed, although a transition state would have a higher energy than a reactant. Figure 4 shows how, with $U = 5.0$eV, three new configurations have appeared; Stage 3 of Ideal and Stages 2 and 3 of NG-1. In Stage 3 of Ideal, the hydrogen has remained attached to the tetrahedral surface and the CO_2 has attached to CH_3CH_2 to form the species $CH_3CH_2COO^-$. This latter species is the initial species of each Stage 2, corresponding to the theory of Almon and Johns where it is attached to the tetrahedral substituted atom, which implies that Ideal, Stage 3 is potentially a real intermediate stage and hence potentially a transition state in decarboxylation. Although Ideal, Stage 3 did not converge to the same criteria as most of the other models, an examination of the distance between the hydrogen atom attached to the tetrahedral surface and the doubly-bonded oxygen of $CH_3CH_2COO^-$ at increasing levels of convergence shows an increase from $3.56\mathring{A}$ to $3.70\mathring{A}$, strongly implying that the $CH_3CH_2COO^-$ species would not move back towards the hydrogen on further convergence. This is strong evidence to suggest that a new intermediate has been identified, and furthermore, it has a higher energy than the Reactant and hence could be a new transition state.

The relaxed geometry of NG-1, Stage 2 is similar to the initial configuration for this stage, except that the species, $CH_3CH_2COO^-$ has moved sufficiently close to the tetrahedral Fe, that a bond is forming between it and an oxygen. An examination of the configuration during the relaxation process showed that the hydrogen of the fatty acid remained attached to the tetrahedral surface. Further relaxation has resulted in the re-attachment of this hydrogen to form the fatty acid and an increase in the

bond length between the Fe on the tetrahedral surface and the oxygen of the fatty acid, from 2.16$\mathring{A}$ to 2.19$\mathring{A}$. Thus, in this case, further relaxation will probably result in the fatty acid detaching from the tetrahedral surface and becoming a variation on the Reactant model configuration, hence it is unlikely to be a new intermediate and hence potential transition state. This was intimated by the negative energy difference between NG-1, Stage 2 and the Reactant.

The relaxed configuration of NG-1, Stage 3 is new to this study and is a variant of a stage hypothesised by Almon and Johns. The energy difference between it and the Reactant is negative and is the largest in magnitude of that between the Reactant and all other models, which would not appear to indicate that it is a transition state between the NG-1 Reactant and Product.

The addition of the Hubbard parameter has changed the Fermi level orbital occupancies as can be seen by comparing Figures 3 and 5. In the case of both Ideal and NG-1 application of GGA-only gives occupation of the Fermi level orbitals within the clay layer, and none at all on any of the interlayer species, which could be due to the correlation effects of the d-orbital electrons of iron. Contrast this with the GGA+U results for both nontronites where, in general there is greater delocalisation of Fermi level occupancy i.e. it extends beyond the irons of the octahedral sheet. In the case of the Reactant model of Ideal, there is no involvement of the clay layer with sole occupation of the fatty acid; in Stage 3 this occupation is on the carboxyl head of the 'new' species, a further indication of its transitory nature. In Stage 2 and the Product models, the Fermi level electrons are within the clay, indicating the relative stability of these interlayer molecules.

For three of the four NG-1 models, application of GGA+U has created some localisation of the Fermi level electrons on the tetrahedral iron and the results for the Reactant model show concentration around the tetrahedral iron and the adjacent oxygens. The degree of confidence with which this environment could be described as a suitable Reactant model has decreased, because the electrons with the highest reactive potential would be expected to exist on the reactive interlayer species. For Stage 2 the Fermi level electrons are localised within the clay layer, around the tetrahedral Fe. If, as suggested in a previous paragraph, further convergence results in separation of the fatty acid from the clay layer, then it is probable the Fermi level occupation remains within the clay. In Stage 3, the highest energy electrons are of the species CH_3CH_2, suggesting this molecule is transitory and yet the negative energy difference between it and the Reactant is the largest within these model sets. This says that, NG-1, Stage 3 could be a possible transition state if there was a positive energy difference between it and the Reactant model, which could be achieved from a different orientation of the Reactant to the clay layer described earlier, where the relaxed orientation of an intermediate produced a Reactant model of lower energy than the original Reactant model. For example, this might apply to the optimised structure of NG-1, Stage 2 as this has a lower energy than the optimised, NG-1 Reactant model, but has the configuration of a potential Reactant model. However, examining the energy differences between NG-1 Stage 3 and NG-1, Stage 2 ($E_{s3} - E_{s2}$) gives an energy difference of -0.272eV, hence the intermediate NG-1, Stage 3 has a lower energy than the optimised NG-1, Stage 2 (reactant configuration) model, and is not a potential transition state of the configurations we have presented. For the

Product model, there is occupation of the clay layer with concentration around the tetrahedral Fe, so, within the previously stated definitions of 'relative stability', the Product model is acceptable as being representative of a final product environment of a decarboxylation pathway.

The difference between Ideal and NG-1 Fermi level occupancies could, in part, be due to the application of the same U value to both octahedral and tetrahedral irons. Table 4 shows that a Hubbard value of 5.0eV has increased the band gaps (in comparison to application of GGA-only) of every configuration apart from Stage 3 of Ideal where there has been an order of magnitude decrease. The band gaps of the NG-1 models are close to that of 1.6eV for $FeSbO_4$ under the GGA+U functional with U = 4eV (Grau-Crespo et al. 2006), where this was found to yield a good description of both magnetic and structural properties of this material.

Application of the Hubbard parameter to Stage 3 of Ideal has reduced its band gap, while, according to the analysis of energy differences and Fermi level orbital occupancies, simultaneously increasing its potential to be a transition state of a decarboxylation reaction within this clay mineral environment. The decrease in band gap indicates that the system is becoming more metallic, and a metallic system requires more k-points than an insulating system to accurately describe the Fermi surface, and too few k-points would contribute to convergence difficulties. So, although Ideal, Stage 3 shows potential to be a transition state in this decarboxylation reaction, further investigation would be required to confirm it as such. For the purposes of this study our goal has been achieved, to determine whether the addition of the Hubbard parameter in DFT+U produces any new potential transition states in comparison to

the application of DFT without the Hubbard parameter.

In summary, two varieties of the iron-bearing clay mineral, nontronite, were examined using GGA and GGA+U to determine whether taking account of the strong correlation between the d-electrons of iron, would result in any new potential transition states within a decarboxylation reaction. The applied Hubbard parameter was determined from a study of wüstite based on the recorded band gap of this material. It was then applied to all iron atoms within all models. The Hubbard parameter increased the band gaps in all but one case (Ideal, Stage 3) but the new band gaps were less than half those of comparable aluminosilicate models. This phenomenon has been reported in another first principles study where the introduction of Fe into aluminosilicate nanotubes reduced the band gap from 4.7eV to 1.4eV (Alvarez-Ramírez 2009).

Employment of the GGA+U functional lead to the identification of three new intermediates, which, when analysed, lead to only one of them — Ideal Stage 3 — being described as a potential transition state of the decarboxylation reaction under examination. It is this model whose band gap *reduced* on application of the Hubbard parameter, which questions the reliability of using band gaps as a guide to counteracting the strong electron correlations, and belies the experimental and theoretical differences in the origins of band gaps. In this instance the d-electron correlations have been addressed with a subsequent decrease in the band gap but the result is, by other methods of analysis, an interesting, new intermediate in the decarboxylation reaction within nontronite.

Our results show that using the Hubbard parameter in DFT for the strongly corre-

lated d-electrons of iron, produces different results to the same calculations carried out without taking account of this phenomenon. As a result of using GGA+U, we have identified a new intermediate in a decarboxylation reaction, which is potentially a transition state. The results obtained from this initial study into the effect of the Hubbard parameter on ferruginous clay minerals, raise questions regarding the reliability of employing a single U value for the same species in different local environments; the relevance of using experimental band gaps as the sole guide to the choice of the U value, and therefore, the requirement to pursue more robust, theoretical methods of accounting for these strongly correlated electrons of the same atomic species within different environments.

ACKNOWLEDGEMENTS

This work made use of the facilities of HECToR, the UK's national high-performance computing service, which is provided by UoE HPCx Ltd at the University of Edinburgh, Cray Inc and NAG Ltd and funded by the Office of Science and Technology through EPSRC's High End Computing Programme. Thanks also to the EPSRC and Durham University's Knowledge Transfer Scheme for funding the work of D Geatches.

References

Almon, W.R. and Johns, W.D. (1975) Petroleum forming reactions: the mechanism and rate of clay catalyzed fatty acid decarboxilation. Proceedings 7^{th} International meeting on organic geochemistry vol. 7th. Wiley, Chichester, 157–171.

Alvarez-Ramírez, F. (2009) First principles studies of Fe-containing aluminosilicate and aluminogermanate nanotubes. Journal of Chemical Theory and Computation, 5, 3224-3231.

Anisimov, V.I., Aryasetiawan, F., and Lichtenstein, A.I. (1997) First-principles calculations of the electronic structure and spectra of strongly correlated systems: the LDA + U method. Journal of Physics: Condensed Matter, 9, 767-808.

Ashcroft, N.W. and Mermin, N.D. (1976) Solid State Physics. Brooks/Cole Thomson Learning Inc.

Branda, M.M., Hernández, N.C., Sanz, J.F., and Illas, F. (2010) Density functional theory study of the interaction of Cu, Ag and Au atoms with the regular CeO_2 (110) surface. Journal of Physical Chemistry C, 114, 1934-1941.

Chen, H.T. and Chang, J.G. (2011) Computational investigation of CO adsorption and oxidation on iron-modified cerium oxide. Journal of Physical Chemistry C, 115, 45-53.

Cococcioni, M., Dal Corso, A., and de Gironcoli, S. (2003) Structural, electronic,

and magnetic properties of Fe_2SiO_4 fayalite: Comparison of LDA and GGA results. Physical Review B, 67, 61-67.

Clark, S.J., Segall, M.D., Pickard, C.J., Hasnip, P.J., Probert, M.J., Refson, K., and Payne, M.C. (2005) Castep v5.0. Zeitschrift für Kristallographie, 220(5-), 567-570.

Devey, A.J., Grau-Crespo, R., and de Leeuw, N.H. (2008) Combined density functional theory and interatomic potential study of the bulk and surface structures and properties of the iron sulfide mackinawite (FeS). Journal of Physical Chemistry C, 112, 60-67.

Devey, A.J., Grau-Crespo, R., and de Leeuw, N.H. (2009) DFT+U study of the iron sulphide mineral greigite (Fe_3S_4) Geochimica et Cosmochimica Acta, 73, A287.

Fang, Z., Solovyev, V., Sawada, H., and Terakura, K. (1999) First-principles study on electronic structures and phase stability of MnO and FeO under high pressure. Physical Review B, 59, 763-773.

Geatches, D.L., Clark, S.J., and Greenwell, H.C. (2010) Role of clay minerals in oil-forming reactions. Journal of Physical Chemistry A, 114, 3569-3575.

Gramsch, S.A., Cohen, R.E., and Savrasov, S.Y. (2003) Structure, metal-insulator transitions, and magnetic properties of FeO at high pressures. American Mineralogist, 88, 257-261.

Grau-Crespo, R., Corà, F., Sokol, A.A., de Leeuw N.H., and Catlow, C.R.A. (2006) Electronic structure and magnetic coupling in $FeSbO_4$: a DFT study using hybrid functionals and GGA + U methods. Physical Review B, 73, 61-69.

Grau-Crespo, R., Catlow, C.R.A., and de Leeuw N.H. (2007) A computer modeling study of redox processes on the $FeSbO_4$ (110) surface. Journal of Catalysis, 248, 77-88.

Greenwood, N.N. and Earnshaw, A. Chemistry of the elements. Pergamon Press, Oxford.

Hernández, N.C., Grau-Crespo, R., de Leeuw, N.H., and Sanz, J.F. (2009) Electronic charge transfer between ceria surfaces and gold adatoms: a GGA+U investigation. Journal of Physical Chemistry Chemical Physics, 11, 46-52.

Hsu, H., Umemoto, K., Wu, Z.Q., and Wentzcovitch, R.M. (2010) Spin-state crossover of iron in lower-mantle minerals: Results of DFT+U investigations Theoretical and Computational Methods in Mineral Physics: Geophysical Applications, 71, 169-199.

Kiejna, A. and Pabisiak, T. (2012) Surface properties of clean and Au or Pd covered hematite (α-Fe_2O_3) (0001) Journal of Physics: Condensed Matter, 24 (095003)1-16.

Kohn, W. and Sham, L.J. (1965) Self-consistent equations including exchange and correlation effects. Physical Review, 140(4A), A1133-A1138.

Kohn, W. and Sham, L.J. (1965) Quantum density oscillations in an inhomogeneous electron gas. Physical Review, 137(6A), A1697-A1705.

Louie, S.G., Froyen, S., and Cohen, M.L. (1982) Nonlinear ionic pseudopotentials in spin-density-functional calculations. Physical Review B, 26, 1738-1742.

Mazari, N., Vanderbilt, D., and Payne, M.C. (1997) Ensemble density functional theory for *ab initio* molecular dynamics of metals and finite-temperature insulators. Physical Review Letters, 79(7), 1337-1340.

Morgan, J.W. and Anders, E. (1980) Chemical composition of Earth, Venus, and Mercury. Proceedings of the National Academy of Sciences, 77, 6973-6977.

Mosey, N.J. and Carter, E.A. (2007) Ab initio evaluation of Coulomb and exchange parameters for DFT+U calculations. Physical Review B, 76, 1551231-15512313.

Nolan, M., Fearon, J.E., and Watson, G.W. (2006) Oxygen vacancy formation and migration in ceria. Solid State Ionics, 177, 3069-3074.

Nolan, M., Elliott, S.E., Mulley, J.S., Bennett, R.A., Basham, M., and Mulheran, P. (2008) Electronic structure of point defects in controlled self-doping of the TiO_2 (110) surface: Combined photoemission spectroscopy and density functional theory study. Physical Review B, 77, (235424)1-11.

Nolan, M. (2012) Charge transfer and formation of reduced Ce^{3+} upon adsorption of metal atoms at the ceria (111) surface Journal of Chemical Physics, 136, (134703)1-9.

Panchmatia, P.M., Sanyal, B., and Oppeneer, P.M. (2007) GGA + U modeling of structural, electronic and magnetic properties of iron porphyrin-type molecules. Journal of Chemical Physics, 343, 47-60.

Perdew, J.P., Burke, K., and Ernzerhof, M. (1996) Generalized gradient approximation made simple. Physical Review Letters, 77(18), 3865-3868.

Pickett, W.E., Erwin, S.C., and Ethridge, E.C. (1998) Reformulation of the LDA + U method for a local-orbital basis. Physical Review B, 58, 1201-1209.

Rák, Zs., Ewing, R.C., and Becker, U. (2011) Role of iron in the incorporation of uranium in optimization garnet matrices. Physical Review B, 84, 155128-15512810.

Rák, Zs., Ewing, R.C., and Becker, U. (2011) First-principles investigation of Ca_3(Ti, Zr, Hf, Sn)$_2Fe_2SiO_{12}$ garnet structure for incorporation of actinides. Physical Review B, 83, 155123-155128.

Stashans, A., Rivera, K., and Pinto, H.P. (2012) First-principles investigations of Fe-doped $MgSiO_3$-ilmenite. Physica B, 407, 2037-2043

Szabová, L., Camellone, M.F., Huang, M., Matolín, V., and Fabris, S. (2010) Thermodynamic electronic and structural properties of Cu/CeO_2 surfaces and interfaces from first-principles DFT+U calculations. Journal of Chemical Physics, 133, (234705)1-11

Vanderbilt, D. (1990) Soft self-consistent pseudopotentials in a generalized eigenvalue formalism. Physical Review B, 41(11), 7892-7895.

Zhou, F., Cococcioni, M., Marianetti, C.A., Morgan, D., and Ceder, G. (2004) First-principles prediction of redox potentials in transition-metal compounds with LDA $+U$. Physical Review B, 70, 21-28.

Figure captions

FIGURE 1. (Color online) On the left is a single unit cell of Ideal containing the product and on the right, a single unit cell of NG-1 containing the reactant. The following colour scheme is used throughout the remainder of this chapter: Oxygen: red; hydrogen: white; aluminium: pink; silicon: yellow; iron: blue; sodium: orange. The dashed line is the periodic boundary of a unit cell.

FIGURE 2. (Color online) A schematic of the intermediate stages in a decarboxylation of a model fatty acid, as theorized by Almon and Johns (1975). The 'R' in the Almon and Johns paper is CH_3 here. These are the pre-optimization stages for both Ideal and NG-1 under each application of the GGA and the GGA+U.

FIGURE 3. (Color Online) Configurations of 1: Ideal and 2: NG-1 models after geometry optimization. The blue shells are the Fermi level orbitals.

FIGURE 4. (Color Online) Relaxed geometries within the GGA+U approximation where $U = 5.0$eV. NG-1, Stage 3 is oriented to show a hydrogen bonded to the basal surface of the clay layer.

FIGURE 5. (Color online) Relaxed geometries within the GGA+U approximation where $U = 5.0$eV. Blue shells are the Fermi level orbitals.

Tables

Models	$E_{s1} - E_r$	$E_{s2} - E_r$	$E_{s3} - E_r$	$E_p - E_r$
Ideal	0.483	-0.310	-0.065	-0.136
NG-1	0.551	-0.722	0.206	-0.168

TABLE 1. Total energy differences (eV) to three significant figures, after geometry optimization under GGA of the nontronite models. $E_{s1,2,3}$ is the energy of stage one, two, three and $E_{r,p}$ is the energy of the Reactant or Product.

Model	Reactant	Stage 1	Stage 2	Stage 3	Product
4	5.10	5.07	5.33	5.11	5.54
Ideal	0.26	0.20	0.19	1.57	0.26
NG-1	1.18	0.16	0.25	0.10	1.10

TABLE 2. Band gaps (eV) of the relaxed clay models where '4' refers to the aluminosilicate Model Set 4 of our previous study (Geatches et al. 2010), i.e. those models contain an all-aluminium octahedral sheet with an Al substitution in the tetrahedral sheet, and a sodium atom in the interlayer space.

Models	$E_{s2} - E_r$	$E_{s3} - E_r$	$E_p - E_r$
Ideal	-0.355	0.833	-0.130
NG-1	-0.323	-0.596	-0.153

TABLE 3. Total energy differences (eV) accurate to three significant figures, after geometry optimization under GGA+U of the nontronite models. $E_{s1,2,3}$ is the energy of stage one, two, three and $E_{r,p}$ is the energy of the Reactant or Product.

Model	Reactant	Stage 1	Stage 2	Stage 3	Product
Ideal	2.17	N/A	2.13	0.05	2.26
NG-1	1.69	N/A	1.53	1.47	1.67

TABLE 4. Band gaps of the relaxed clay models within the GGA+U approximation with $U = 5.0$eV.

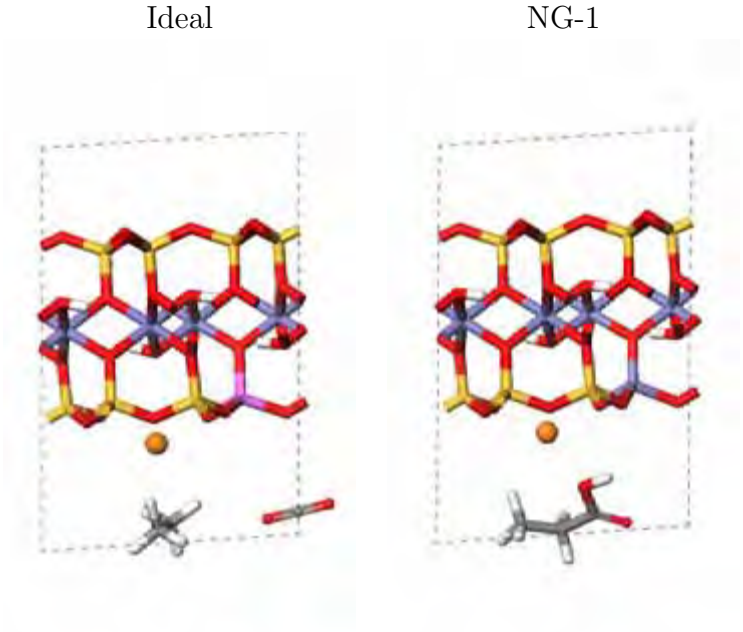

FIGURE 1. (Color online) On the left is a single unit cell of Ideal containing the product and on the right, a single unit cell of NG-1 containing the reactant. The following colour scheme is used throughout the remainder of this chapter: Oxygen: red; hydrogen: white; aluminium: pink; silicon: yellow; iron: blue; sodium: orange. The dashed line is the periodic boundary of a unit cell.

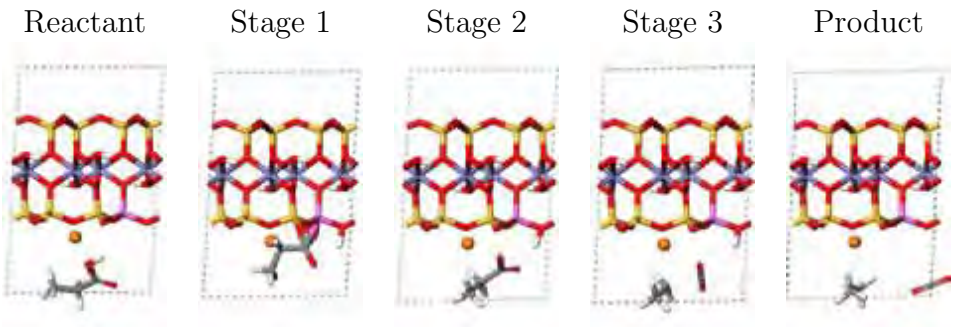

FIGURE 2. (Color online) A schematic of the intermediate stages in a decarboxylation of a model fatty acid, as theorized by Almon and Johns (1975). The 'R' in the Almon and Johns paper is CH_3 here. These are the pre-optimisation stages for both Ideal and NG-1 under each application of the GGA and the GGA+U.

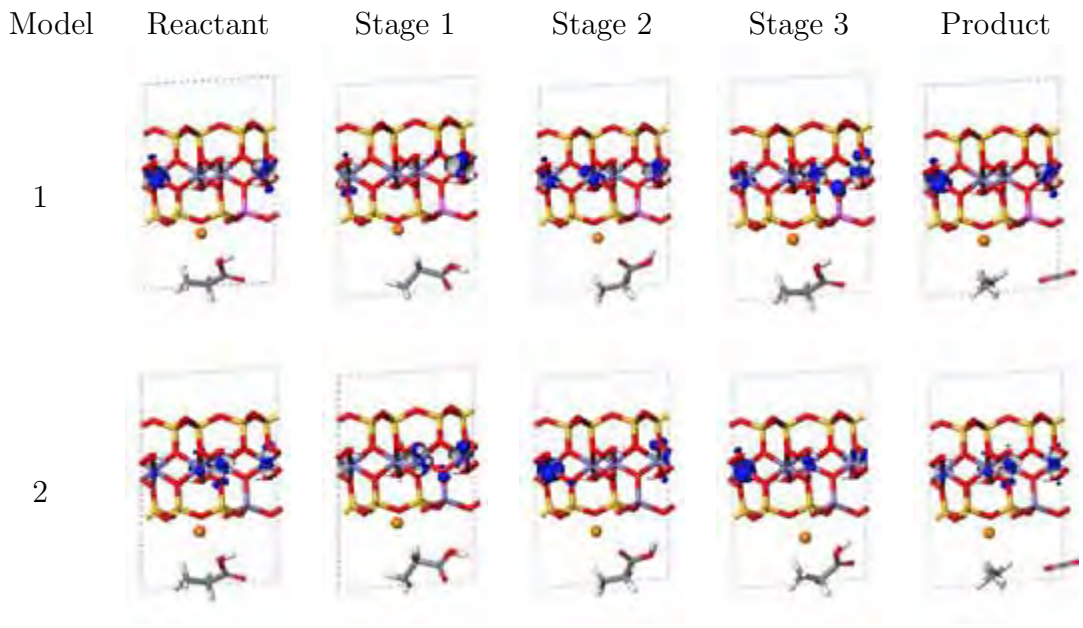

FIGURE 3. (Color Online) Configurations of 1: Ideal and 2: NG-1 models after geometry optimisation. The blue shells are the Fermi level orbitals.

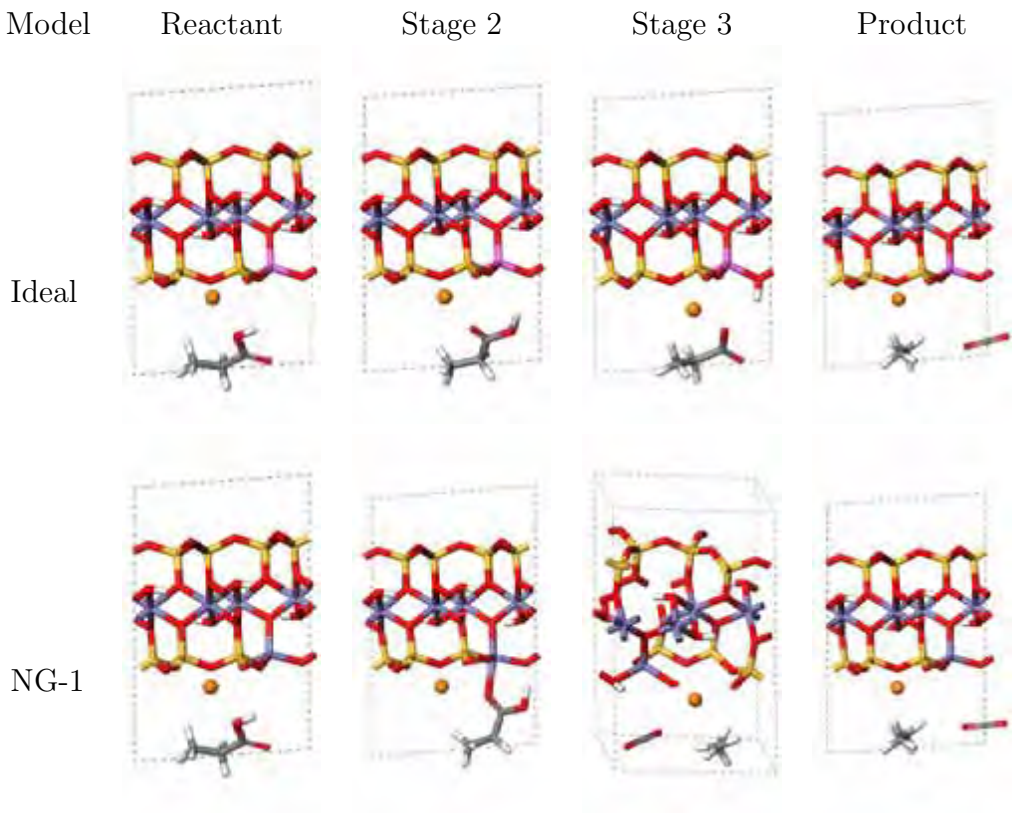

FIGURE 4. (Color Online) Relaxed geometries within the GGA+U approximation where $U = 5.0$eV. NG-1, Stage 3 is oriented to show a hydrogen bonded to the basal surface of the clay layer.

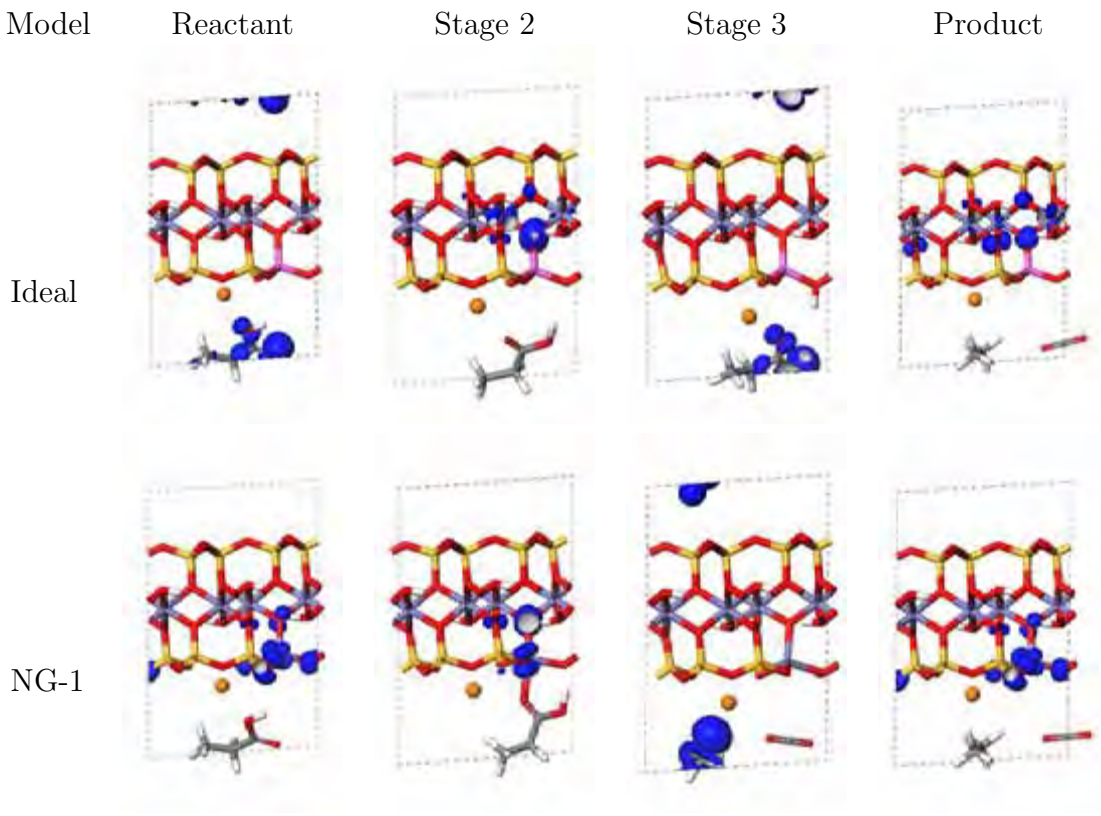

FIGURE 5. (Color online) Relaxed geometries within the GGA+U approximation where $U = 5.0$eV. Blue shells are the Fermi level orbitals.